Driven inelastic-particle systems with drag

Jonathan J. Wylie, Qiang Zhang, and Yun Li
Department of Mathematics, City University of Hong Kong, Tat Chee Avenue, Kowloon, Hong Kong

Xu Hengyi
Condensed Matter Physics Laboratory, Heinrich-Heine-Universititat, Universitatsstrasse 1, 40225 Dusseldorf, Germany

(Received 26 September 2008; revised manuscript received 28 November 2008; published 11 March 2009)

We study steady states of the motion of a large number of particles in a closed box that are excited by a vibrating boundary and experience a linear drag force from the interstitial fluid. The dissipation in such systems arises from two main sources: Inelasticity in particle collisions and the effects of interstitial fluid on the particles. In many applications, order of magnitude estimates suggest that the dissipation due to interstitial fluid effects may greatly exceed that due to inelasticity and one is naturally led to neglect inelastic effects. In this study, we show that, if one adopts a linear drag force and inelastic effects are neglected, a steady state only exists when the vibration speed of the boundary is below a critical value. For vibration speeds above this critical value, no steady state exists since the kinetic energy of the particles grows without bound. We show that, for vibration speeds above the critical value, inelastic effects must be included to obtain a steady state even if order of magnitude estimates suggest they are negligible. Numerical simulations confirm these theoretical predictions. We also show that inclusion of apparently small nonlinear drag terms can also play a similar role in preventing the kinetic energy of the particles growing without bound.

DOI: 10.1103/PhysRevE.79.031301 PACS number(s): 45.70.−n

I. INTRODUCTION

Many industrial applications require large numbers of discrete solid particles to be transported and processed. In general, these particles are surrounded by a fluid. These systems are subject to two main sources of energy dissipation: Inelasticity in particle collisions, and the effects of the interstitial fluid. For dense flows made up of large particles suspended in a gas (such as rock avalanches), the dissipation due to the interstitial fluid will be negligible and dissipation will be dominated by the effects of inelasticity. However, in many cases, such as fluidized beds, sediment transport and slurry flows, the interstitial fluid can play a crucial role in determining the dissipation.

In the absence of any external energy sources, the highly dissipative nature of these systems mean that the particles rapidly come to rest. However, if sufficiently large amounts of energy are supplied, the particles can become highly agitated and the material can adopt a state that is similar to a kinetic gas. In a wide range of applications the particles obtain the energy to achieve this agitated state via interactions with boundaries. In many industrial processes this occurs through mechanical forcing in which vibrating boundaries impart kinetic energy to the particles in its vicinity. Such forcing has been studied in a variety of contexts by a number of authors [1–9].

For vibrated systems, the case in which the dissipation is dominated by inelastic effects has been widely studied. However, the case in which the dissipation due to the interstitial fluid is important has received much less attention. This is perhaps surprising since there are a wide range of important physical processes in which the overall dissipation is dominated by drag from the interstitial fluid [10]. Kumaran [4] considered a system of particles in an open box with a vibrated base and included the effects of gravity. Among a number of important results, he showed that steady states could always be determined when the dissipation is dominated by interstitial fluid effects and the dissipation due to inelastic collisions are neglected. Various authors [11–14] considered a binary mixture of spheres of different density and equal radius that are vibrated and experience a drag force from the interstitial fluid and showed that surprising segregation effects can occur.

In this paper, we will consider a system of particles in a closed box with energy added to the system by a vibrating boundary. In many applications, order of magnitude estimates suggest that the dissipation due to interstitial fluid effects may greatly exceed that due to inelasticity. Therefore, one may be led to neglect inelastic effects. We will therefore determine the conditions under which dissipation due to a linear drag force from the interstitial fluid can balance the energy input from the boundary forcing and hence maintain a steady state. We will use equations based on kinetic theory to perform a theoretical analysis of such systems. Surprisingly, when inelastic effects are neglected, we will show that a steady state can only exist if the vibration speed of the boundary is below a critical value. For vibration speeds above this critical value, the kinetic energy of the particles grows without bound. However, if inelastic effects are included, we show that a steady state can be achieved even for vibration speeds above the critical value. Therefore, above the critical vibration speed, inelastic effects must be included even though order of magnitude estimates suggest they are negligible. We provide analytical expressions for the critical vibration speed. For elastic systems we also determine the asymptotic behavior of the system for vibration speeds near the critical value. We also determine the asymptotic behavior for large vibration speeds when inelastic effects are included. We conduct three-dimensional numerical simulation for both elastic- and inelastic-particle systems and show that the results from numerical simulation give good qualitative agreement with our theoretical predictions. We also show that the

inclusion of nonlinear drag terms, even though they appear to be small can also prevent the kinetic energy of the particles to grow without bound.

The rest of the paper will be organized as follows: In Sec. II, we present the theoretical formulation for the equations which govern the steady state. In Sec. III, we use a simple model for the energy input from the vibrating boundary and derive the solution for the steady state when inelastic effects are neglected. We show that the pressure tends to infinity as the vibration speed tends to a critical value from below. In Sec. IV, we show that if the inelasticity in particle collisions is included in the theoretical analysis, then a steady state will always exist even if the vibration speed exceeds the critical value. In Sec. V, we present the result of numerical simulations which confirm the theoretical predictions presented in Sec. III. In Sec. VI we consider the effects of nonlinear drag. In Sec. VII we present a summary of our findings. In Appendix A we give details of some of the constitutive models used to demonstrate the phenomena described in this paper. In Appendix B, we show that the same phenomena occurs when we take a more detailed approach to modeling the energy input from the vibrating boundary [2].

II. THEORETICAL FORMULATION

We consider a system that contains a large number of identical smooth spherical particles with radius a and density ρ. The particles are confined between two parallel smooth and rigid boundaries. One of the boundaries vibrates in the direction perpendicular to its own plane, while the other boundary is fixed. The mean separation between the two boundaries is L. We denote the mean fraction of the volume occupied by the particles as $\bar{\phi}$. The masses of both of the walls are considered to be sufficiently larger than the masses of the particles that collisions between particles and boundaries have a negligible effect on the motion of the boundaries. For simplicity, we adopt a "saw-tooth" motion for the vibrating boundary [8,15], in which the wall moves with a constant speed w over a distance d before executing an instantaneous jump back to its starting position. We further assume that $d \ll L$, and so, to the leading order, all collisions with the vibrating boundary occur at the same location. This assumption avoids the presence of heat pulses that propagate away from the wall [8] and allows the possibility of genuine steady states. Figure 1 shows the basic setting of this system.

When two particles collide or when a particle collides with the wall, the velocities are updated using the standard collision rules with a constant coefficient of restitution e. Between particle collisions the particles simply obey Newton's second law and experience drag due to the interstitial fluid. We will assume that the drag $\mathbf{F}_d$, experienced by the particles, can be approximated by a Stokes drag law

$$\mathbf{F}_d = -6\pi\mu a\mathbf{u},$$

where μ is the viscosity of the fluid and $\mathbf{u}$ is the velocity of the individual particles. If the local volume fraction of particles is large, this force can be enhanced by the presence of neighboring particles. This effect has been studied by Sangani *et al.* [16] who showed that the dissipation arising from viscous drag must be multiplied by a function of the local volume fraction. For simplicity we neglect this effect, although the inclusion of this effect does not qualitatively effect the results that we present here. The use of the Stokes drag law requires that the inertia as measured by the Reynolds number based on the particle radius is small. Order of magnitude estimates suggest that this requires that

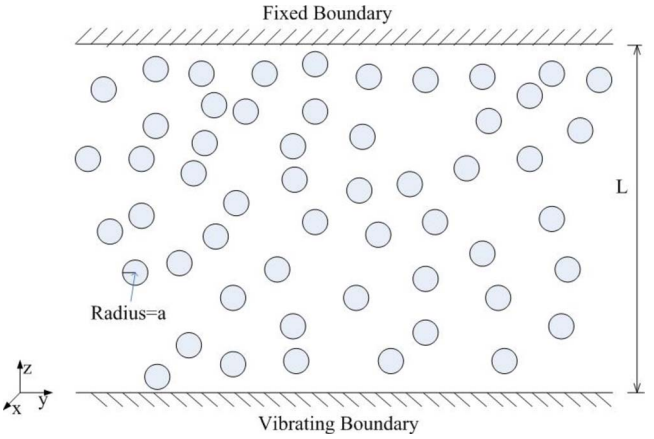

FIG. 1. (Color online) Schematic of the system.

$$\mathrm{Re} = \frac{\rho_f a w}{\mu} \ll 1,$$

where ρ_f is the density of the interstitial fluid. We will revisit the validity of this assumption of using the Stokes drag law and study the effect of nonlinear drag in Sec. VI.

If suspensions are sufficiently energetic then the trajectories of the particles between collisions are only weakly affected by the fluid drag. In addition, if particle collisions are not too dissipative, then it can be shown that the particles obtain an approximately Maxwellian distribution and behave similarly to a kinetic gas [10].

As in kinetic gas theory, we separate the motion of particles into mean flow $\mathbf{U}=\langle\mathbf{u}\rangle$ and fluctuation $\mathbf{u}-\mathbf{U}$ where the angular brackets represent the local average over particles in the suspension. The variance of the velocity fluctuation gives the granular temperature,

$$T = \tfrac{1}{3}\langle(\mathbf{u}-\langle\mathbf{u}\rangle)\cdot(\mathbf{u}-\langle\mathbf{u}\rangle)\rangle.$$

Continuum equations that govern such systems have been developed by a number of authors [16–20]. The general form of the equations is

$$\frac{D(\rho\phi)}{Dt} + \rho\phi\nabla\cdot\mathbf{U} = 0,$$

$$\rho\phi\frac{D\mathbf{U}}{Dt} = \nabla\cdot\boldsymbol{\Sigma} - \frac{9\phi\mu}{2a^2}\mathbf{U},$$

$$\frac{3\rho\phi}{2}\frac{DT}{Dt} = -\nabla\cdot\mathbf{q} + \boldsymbol{\Sigma}:\nabla\mathbf{U} - \Gamma_{\mathrm{vis}} - \Gamma_{\mathrm{inelas}}, \tag{1}$$

where $\frac{D}{Dt}=\frac{\partial}{\partial t}+\mathbf{U}\cdot\nabla$ is the material derivative operator and ϕ is the local volume fraction. To avoid confusion, we note that

ρ represents the mass density of the material of which the particles are composed, whereas the density of the granular gas is given by $\rho\phi$. The quantities $\boldsymbol{\Sigma}$, $\mathbf{q}$, Γ_{vis} and Γ_{inelas} denote the stress tensor, the fluctuation energy flux, the rate of energy dissipation due to the viscous drag and the rate of energy dissipation due to inelasticity in collisions, respectively. The equations (1) represent the balance of mass, momentum, and energy, respectively. The dissipation due to viscous drag takes the form

$$\Gamma_{\text{vis}} = \frac{\mu T}{a^2}\Gamma_1(\phi), \tag{2}$$

and the dissipation due to inelasticity in particle collisions takes the form

$$\Gamma_{\text{inelas}} = \frac{(1-e^2)\rho T^{3/2}}{a}\Gamma_2(e,\phi), \tag{3}$$

where Γ_1 and Γ_2 are dimensionless functions that can be derived from kinetic theory. Here, and in what follows, we take the approach of Sangani *et al.* [16] in assuming that the inelastic dissipation rate, the particle stress tensor and other transport coefficients are only weakly affected by the fluid drag force.

For general flows the constitutive laws that relate the stress and energy flux to the state of the suspension are rather complicated, but we will consider steady states in which there must be no net flow. Therefore, terms involving temporal derivatives and spatial gradients in the horizontal directions vanish and the mean velocity is zero everywhere. In this case, the fluctuation flux $\mathbf{q}$ has no horizontal components and the component in the vertical direction, q_z, can be expressed as

$$q_z = -\left(\kappa\frac{dT}{dz} + \eta\frac{d\phi}{dz}\right), \tag{4}$$

where κ is the thermal conductivity of the fluctuation energy, and η is the mass diffusion coefficient. Equation (4) shows that two factors contribute to transferring energy: Thermal conduction and mass diffusion.

Under the assumptions discussed above, (1) has the following form:

$$\frac{dp}{dz} = 0, \tag{5}$$

$$\frac{d}{dz}\left(\kappa\frac{dT}{dz} + \eta\frac{d\phi}{dz}\right) = \Gamma_{\text{vis}} + \Gamma_{\text{inelas}}, \tag{6}$$

where p is the kinetic pressure of the particles. Expressions for the quantities p, κ, and η are given by kinetic theory

$$p = \rho T F(\phi), \tag{7}$$

$$\kappa = \rho a T^{1/2}\kappa_1(e,\phi), \tag{8}$$

$$\eta = \rho a T^{3/2}\eta_1(e,\phi), \tag{9}$$

where $F(\phi)$, $\kappa_1(e,\phi)$, and $\eta_1(e,\phi)$ are dimensionless functions. Various studies have been carried out in the literature to derive the transport coefficients $\Gamma_1(\phi)$, $\Gamma_2(e,\phi)$, $F(\phi)$, $\kappa_1(e,\phi)$, and $\eta_1(e,\phi)$ under different assumptions. We list some of the expressions for these quantities from the literature in Appendix A. In the theoretical analysis presented in this paper, we will keep these functions in their general form. Only when we plot the numerical results, we will demonstrate them with the specific functional forms listed in the Appendix A.

We note that freely cooling granular gases form dense clusters [21] that have raised doubts about the adequacy of the equations given above. However, for driven particle systems the formation of clusters is often heavily reduced by the driving. In driven systems, hydrodynamic descriptions have been extremely widely used and good agreement with numerical simulations and experiments has been found [2,3,5,7,22]. Moreover, for elastic particles that experience drag, Wylie and Koch [10] showed a hydrodynamic description can give good agreement with simulations.

Equation (5) is a first-order ordinary differential equation and Eq. (6) is a second-order ordinary differential equation, therefore we need three conditions to specify the system. The first condition is that the average volume fraction $\bar{\phi}$ in the system is fixed, which gives

$$\frac{1}{L}\int_0^L \phi(z)dz = \bar{\phi}. \tag{10}$$

The remaining two conditions come from the rate of change of energy due to particle collisions with the walls, which are given by

$$q_z|_{z=L} = -\rho\phi_L\int_{\mathbf{u}\cdot\hat{\mathbf{z}}>0} u_z\frac{\Delta E_L}{m}f_L(\mathbf{u})d\mathbf{u} \tag{11}$$

and

$$q_z|_{z=0} = \rho\phi_0\int_{\mathbf{u}\cdot\hat{\mathbf{z}}<0} -u_z\frac{\Delta E_0}{m}f_0(\mathbf{u})d\mathbf{u}. \tag{12}$$

Here ϕ_L (ϕ_0) is the local volume fraction at $z=L$ ($z=0$), m is the mass of the particles, $\hat{\mathbf{z}}$ is the unit vector in the z direction, u_z is the velocity component perpendicular to the wall, and f_L (f_0) is the velocity distribution at $z=L$ ($z=0$). $\Delta E_L = -\frac{1-e_w^2}{2}mu_z^2$ is the energy loss per particle collision with the fixed wall, where e_w is the coefficient of restitution for collisions between particles and walls. $\Delta E_0 = \frac{m}{2}\{[(1+e_w)w - e_w u_z]^2 - u_z^2\}$ is the energy gain per particle collision with the vibrating wall.

Equation (5) gives that pressure is a constant, i.e.,

$$p = P, \tag{13}$$

where P is a constant to be determined later. Then from (7) and (13), we have $\rho F(\phi)T = P$. Using this expression to eliminate the temperature from the energy equation (6) yields

$$-\frac{d}{dz}\left(J(\phi)\frac{d\phi}{dz}\right) = S_1 K_1(\phi)P^{-1/2} + (1-e^2)S_2 K_2(e,\phi),$$

$$z \in (0,L) \tag{14}$$

with boundary conditions

$$J(\phi)\frac{d\phi}{dz} = P^{-3/2}a^{-1}\sqrt{\rho}Q_L \quad \text{at } z = L \tag{15}$$

and

$$J(\phi)\frac{d\phi}{dz} = P^{-3/2}a^{-1}\sqrt{\rho}Q_0 \quad \text{at } z = 0, \tag{16}$$

where

$$J(\phi) = \frac{\kappa_1(e,\phi)}{F^{5/2}(\phi)}\frac{dF(\phi)}{d\phi} - \frac{\eta_1(e,\phi)}{F^{3/2}(\phi)},$$

$$S_1 = \frac{\mu}{\sqrt{\rho}a^3}, \quad K_1(\phi) = \frac{\Gamma_1(\phi)}{F(\phi)},$$

$$S_2 = \frac{1}{a^2}, \quad K_2(\phi) = \frac{\Gamma_2(e,\phi)}{F^{3/2}(\phi)},$$

$$Q_L = \rho\phi_L\int_{\mathbf{u}\cdot\hat{\mathbf{z}}>0}\frac{(1-e_w^2)}{4}u_z^3 f_L(\mathbf{u})d\mathbf{u}, \tag{17}$$

and

$$Q_0 = \rho\phi_0\int_{\mathbf{u}\cdot\hat{\mathbf{z}}<0} -\frac{u_z}{2}\{[(1+e_w)w - e_w u_z]^2 - u_z^2\}f_0(\mathbf{u})d\mathbf{u}. \tag{18}$$

In order to evaluate the integrals in (17) and (18), one needs to have detailed information about the velocity distributions at the two walls, f_0 and f_L. At the vibrating wall, the nature of the boundary condition implies that there will be significant deviations from a Maxwellian distribution. A detailed study of the distribution requires the solution of the kinetic equation which is beyond the scope of this study. A number of previous authors have been faced with a similar problem and a number of models that couple the energy input from the boundary to the particles in the interior have been developed. Warr and Huntley [9] proposed a model in which the distribution was approximated by a Maxwellian. Later, Kumaran [4] showed that one could indeed use the Maxwellian distribution to evaluate the integrals if one considered the asymptotic limit in which the typical velocity of particles is much smaller than velocity of the vibrating wall. The approach of using a Maxwellian distribution has also been used by Eggers [3] who found reasonable agreement with simulations. A more detailed study has been performed by Brey *et al.* [2] who analyzed a model for the distribution function that is consistent with the vibrating boundary. In this paper, we will consider both the approach of using a Maxwellian approximation used by [3,4,9] and the more detailed approach used by Brey *et al.* [2]. In the interests of readability, we will first present all theoretical results based on Maxwellian approximation. The corresponding results based on the approach of Brey *et al.* [2] are given in Appendix B. We show that both approaches give the same qualitative results.

Based on the assumptions that f_L and f_0 are approximately Maxwellian, (17) and (18) can be written as

$$Q_L = \frac{1-e_w^2}{2}\rho\phi_L\sqrt{\frac{2P^3}{\pi[\rho F(\phi_L)]^3}}, \tag{19}$$

and

$$Q_0 = \frac{1+e_w}{2}\rho\phi_0\left((1+e_w)w^2\sqrt{\frac{P}{2\pi\rho F(\phi_0)}} + e_w w\frac{P}{\rho F(\phi_0)} - (1-e_w)\sqrt{\frac{2P^3}{\pi[\rho F(\phi_0)]^3}}\right). \tag{20}$$

Here we have used the fact that $T_L = P/[\rho F(\phi_L)]$ and $T_0 = P/[\rho F(\phi_0)]$. The steady state of our system is completely determined by the differential equation (14) with boundary conditions (15) and (16), the constraint on volume fraction (10) and the expressions for Q_L and Q_0 are given by (19) and (20).

III. THEORY WHEN INELASTIC EFFECTS ARE NEGLECTED

Order of magnitude estimates show that the dissipation due to interstitial fluid effects will greatly exceed the dissipation due to inelasticity if $\frac{4\bar{\phi}(1-e^2)\rho a w}{9\sqrt{\pi}\mu} \ll 1$. In these cases, it seems natural to neglect the dissipation due to inelasticity and consider the behavior of elastic-particle systems. However, we will show that inelastic effects can only be neglected for values of the wall vibration speed below a critical value. For vibration speeds exceeding the critical value, no steady state exists and the effects of inelasticity must be included even though order of magnitude estimates suggest they are negligible.

Furthermore, we will determine the conditions under which boundary forcing can maintain a highly agitated state in a discrete particle system in which the interstitial fluid plays a dominant role in the overall dissipation. We use the system pressure P to measure how agitated the particle system is, and determine the relationship between P and the speed of vibrating boundary w which measures the magnitude of external energy input.

For $e=1$ and $e_w=1$, the differential equation (14) becomes

$$\frac{d}{dz}\left(J(\phi)\frac{d\phi}{dz}\right) = -S_1K_1(\phi)P^{-1/2}. \tag{21}$$

The constraint on volume fraction is given by (10). The boundary conditions (15) and (16) become

$$J(\phi)\frac{d\phi}{dz} = 0 \quad \text{at } z = L, \tag{22}$$

$$J(\phi)\frac{d\phi}{dz} = P^{-3/2}a^{-1}\sqrt{\rho}Q_0 \quad \text{at } z = 0, \tag{23}$$

where, cf. (20),

$$Q_0 = wP\frac{\phi_0}{F(\phi_0)}\left(1 + w\sqrt{\frac{2\rho F(\phi_0)}{\pi P}}\right). \tag{24}$$

Here we have applied the fact that $Q_L=0$ when $e_w=1$.

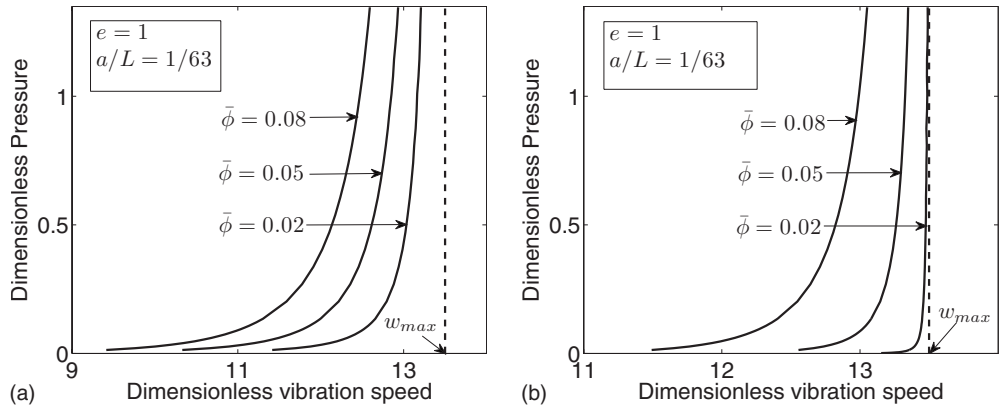

FIG. 2. The dimensionless pressure $P/(\frac{\mu^2 L^4}{\rho a^6})$ is plotted against the dimensionless wall velocity $w/(\frac{\mu L}{\rho a^2})$ for elastic-particle systems $(e=1)$, $a/L=1/63$ and various mean volume fractions. There exists a critical value of the wall velocity $w_{\max}$ for which the pressure tends to infinity. For values of the wall velocity exceeding the critical value, no steady solution exist. (a) Maxwellian approximation near boundaries and constitutive laws (A1)–(A6); (b) the Brey *et al.* [2] model near boundaries and constitutive laws (A7)–(A16).

A. Parametric solution

Our purpose is to determine the pressure P for a given mean volume fraction $\bar{\phi}$ and a vibration speed w. The system given by (10) and (21)–(24) contains a highly nonlinear second-order ordinary differential equation. In spite of the highly nonlinear nature of the problem, we will derive a closed-form solution in parametric form. More specifically, we will derive expressions for P, $\bar{\phi}$, and w in terms of ϕ_0 and ϕ_L.

Multiplying both sides of (21) by $J(\phi)\frac{d\phi}{dz}$ and integrating from ϕ to ϕ_L, we obtain

$$\frac{d\phi}{dz} = (2S_1)^{1/2} P^{-1/4} \frac{1}{J(\phi)} \left(\int_{\phi}^{\phi_L} K_1(\phi') J(\phi') d\phi' \right)^{1/2}. \tag{25}$$

Here we have used the boundary condition at $z=L$ and the fact $J(\phi)\frac{d\phi}{dz} \geqslant 0$. The above equation allows us to determine z as a function of ϕ by integrating from ϕ_0 to $\phi(z)$,

$$z = (2S_1)^{-1/2} P^{1/4} \int_{\phi_0}^{\phi} J(\phi'') \left(\int_{\phi''}^{\phi_L} K_1(\phi') J(\phi') d\phi' \right)^{-1/2} d\phi''.$$

At $z=L$, we have $\phi=\phi_L$, and the above equation gives P in terms of ϕ_0 and ϕ_L,

$$P^{-1/4} = (2S_1 L^2)^{-1/2} \int_{\phi_0}^{\phi_L} J(\phi'') \left(\int_{\phi''}^{\phi_L} K_1(\phi') J(\phi') d\phi' \right)^{-1/2} d\phi''. \tag{26}$$

The constraint on the volume fraction (10) can be written as

$$\bar{\phi} = \frac{1}{L} \int_{\phi_0}^{\phi_L} \phi \frac{dz}{d\phi} d\phi. \tag{27}$$

Substituting (25) and (26) into (27), we obtain $\bar{\phi}$ as a function of ϕ_0 and ϕ_L,

$$\bar{\phi} = \frac{\displaystyle\int_{\phi_0}^{\phi_L} \phi'' J(\phi'') \left(\int_{\phi''}^{\phi_L} K_1(\phi') J(\phi') d\phi' \right)^{-1/2} d\phi''}{\displaystyle\int_{\phi_0}^{\phi_L} J(\phi'') \left(\int_{\phi''}^{\phi_L} K_1(\phi') J(\phi') d\phi' \right)^{-1/2} d\phi''}. \tag{28}$$

Evaluating (25) at point $z=0$, and substituting the result into (23), we obtain

$$Q_0 = P^{5/4} \left(\frac{2a^2 S_1}{\rho} \int_{\phi_0}^{\phi_L} K_1(\phi') J(\phi') d\phi' \right)^{1/2}. \tag{29}$$

Substituting (26) into (29), we obtain

$$Q_0 = \rho^{-1/2} a (2S_1)^3 L^5 \times \frac{\left(\displaystyle\int_{\phi_0}^{\phi_L} K_1(\phi') J(\phi') d\phi' \right)^{1/2}}{\left[\displaystyle\int_{\phi_0}^{\phi_L} J(\phi'') \left(\int_{\phi''}^{\phi_L} K_1(\phi') J(\phi') d\phi' \right)^{-1/2} d\phi'' \right]^5}. \tag{30}$$

Therefore, (26), (28), and (30), provide us with expressions for P, $\bar{\phi}$, and Q_0 in terms of parameters ϕ_0 and ϕ_L.

Now, we relate w to ϕ_0 and ϕ_L. Equation (24) is a quadratic equation for w which has two roots. The only positive root is

$$w = \frac{F(\phi_0) Q_0 / P \phi_0}{1/2 + \sqrt{1/4 + \sqrt{2\rho F^{3/2}(\phi_0) Q_0^2 / (P^3 \phi_0^2)}}}. \tag{31}$$

Since P and Q_0 are given by (26) and (30) as functions of ϕ_0 and ϕ_L, it follows that (31) gives us an expression for w in terms of ϕ_0 and ϕ_L.

Equations (26) and (30) show that P and Q_0 scale as $\frac{\mu^2 L^4}{\rho a^6}$ and $\frac{\mu^3 L^5}{\rho^2 a^8}$, respectively. Equation (31) shows that for fixed a/L, w scales as $\frac{\mu L}{\rho a^2}$. The dependence on a/L comes from the term Q_0^2/P^3 in the denominator of (31). Based on these parametric forms, we plot the dimensionless pressure $P/(\frac{\mu^2 L^4}{\rho a^6})$ as

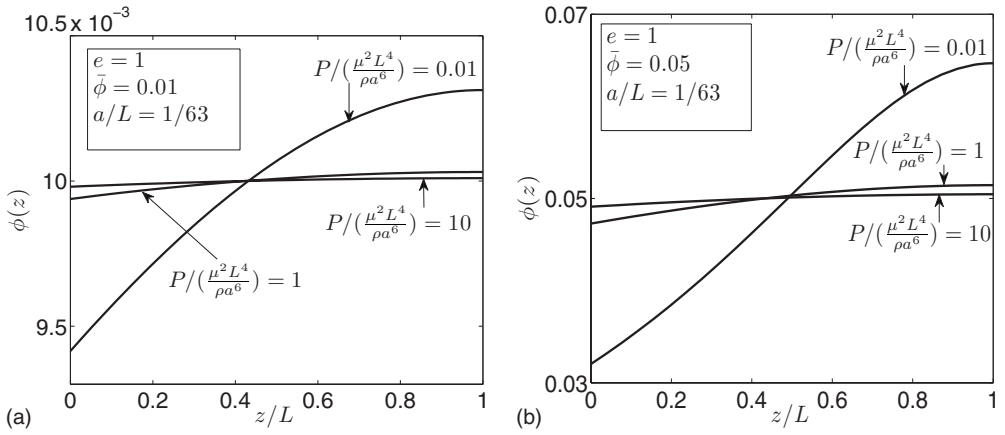

FIG. 3. The local volume fraction $\phi(z)$ is plotted against z/L for elastic-particle systems ($e=1$) under different pressures. (a) $\bar{\phi}=0.01$; (b) $\bar{\phi}=0.05$. The volume fraction profile becomes more uniform as pressure increases. The constitutive model (A1)–(A6) is used for both (a) and (b).

a function of the dimensionless vibration speed $w/(\frac{\mu L}{\rho a^2})$ for $a/L=1/63$ and various values of $\bar{\phi}$ [see Fig. 2(a)]. In Fig. 2(a), we present results using the model (19) and (20) for energy flux through the boundaries that assumes that the velocity distributions near the boundaries are approximately Maxwellian. In this figure we use the model for the constitutive relations (A1)–(A6) that is valid for $1-e \ll 1$ and over a large range of volume fractions. To show that our results are qualitatively insensitive to the choice of model we also present results for alternative models for both the energy flux through the boundaries and the constitutive relations. In Fig. 2(b) we present results based on the more detailed approach of modeling the energy flux through the vibrating boundary by Brey *et al.* [2] (its derivation is given in Appendix B). In this figure we use the model for constitutive relations (A7)–(A16) that include high-order corrections in e, but neglect the effects of high volume fractions. We will follow the same approach in presenting the results for these two models in (a) and (b) of Figs. 4, 5, 7, 8, 10, 12, and 13.

Figure 2 shows that, for each fixed $\bar{\phi}$, there is a maximum wall speed $w_{\max}$ at which the pressure becomes infinitely large and above which no steady-state solution exists. This is true for both the Maxwellian approximation and the Brey *et al.* approximation for the energy flux at the boundary.

In Fig. 3, we plot the local volume fraction as a function of the distance from the vibrating boundary. Near the vibrating boundary, where the energy is input, the particles have higher temperature than particles that are further away from the vibrating boundary. Since the system pressure is constant, the particles near this vibrating boundary must have lower volume fraction. So the volume fraction increases monotonically with the distance from the vibrating boundary. As the pressure increases, the volume fraction becomes more uniform and for large values of the pressure, there are only very small differences in the volume fraction.

Figure 2 shows that there is a critical vibration speed $w_{\max}$. For $w>w_{\max}$, no steady state exists. Physically, this occurs for the following reason: As w increases, the energy that each particle obtains from colliding with the vibrating wall increases. This tends to increase the temperature near the vibrating wall and so the particles collide more rapidly with the wall. Both of these effects cause the rate of energy input to increase dramatically as w increases. As w approaches $w_{\max}$, it becomes increasingly difficult for the drag to dissipate all of the energy that is input. For $w>w_{\max}$, the drag can no longer match the rate of energy input and the energy of system continuously increases. Hence, no steady state can be obtained for $w>w_{\max}$.

In the following section, we analyze the behavior of the system near this critical wall speed $w_{\max}$.

B. Asymptotic solution near $w_{\max}$

When the velocity of the vibrating boundary is very close to $w_{\max}$, the pressure of the system will be large and the volume fraction will be approximately uniform (see Fig. 3). This also can be seen by taking the limit $P\to\infty$ in (26) which implies $\phi_L\to\phi_0$. Therefore, $\phi_L-\phi$ is small for all $\phi \in (\phi_0,\phi_L)$. We now expand the parametric solution in terms of this small parameter to obtain the explicit asymptotic behavior of P as a function of $\bar{\phi}$ and w.

Equation (25) can be written as

$$\frac{d(\phi_L-\phi)}{dz} = -\frac{d\phi}{dz} = P^{-1/4}\left(\frac{2S_1K_1(\phi_L)}{J(\phi_L)}(\phi_L-\phi)\right)^{1/2} \times\left[1+\left(\frac{3J'(\phi_L)}{4J(\phi_L)}-\frac{K_1'(\phi_L)}{4K_1(\phi_L)}\right)(\phi_L-\phi) + O[(\phi_L-\phi)^2]\right]. \tag{32}$$

Equation (32) can be solved explicitly and the result is given by

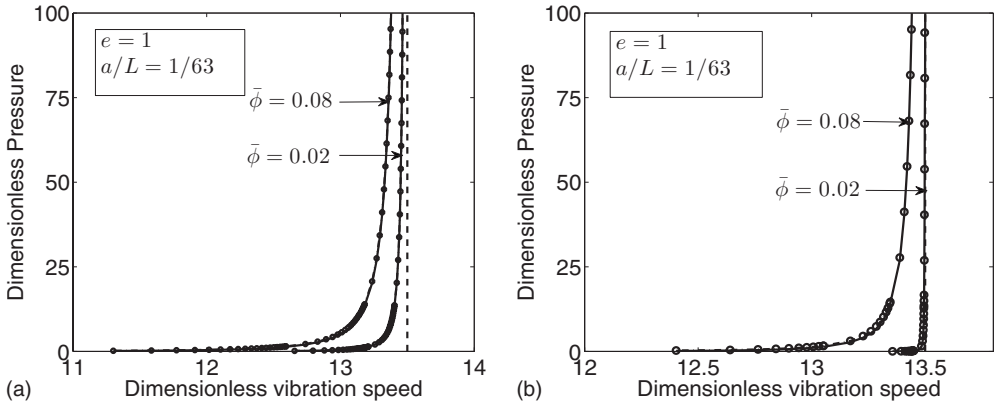

FIG. 4. The dimensionless pressure $P/(\frac{\mu^2 L^4}{\rho a^6})$ is plotted against the dimensionless wall velocity $w/(\frac{\mu L}{\rho a^2})$ when w is near $w_{\max}$ for elastic-particle systems ($e=1$) and various mean volume fractions. The dashed line is the location of dimensionless $w_{\max}/(\frac{\mu L}{\rho a^2})$. The asymptotic solution (dots) is in good agreement with the general solution (solid curve) when pressure is large. (a) Maxwellian approximation near boundaries and constitutive laws (A1)–(A6); (b) the Brey *et al.* [2] model near boundaries and constitutive laws (A7)–(A16).

$$\sqrt{\phi_L - \phi} = P^{-1/4}\left(\frac{S_1 K_1(\phi_L)}{2J(\phi_L)}\right)^{1/2}(L-z)\left[1 + \frac{1}{3}P^{-1/2}\left(\frac{3J'(\phi_L)}{4J(\phi_L)} - \frac{K_1'(\phi_L)}{4K_1(\phi_L)}\right)\frac{S_1 K_1(\phi_L)}{2J(\phi_L)}(L-z)^2 + O(P^{-1})\right]. \quad (33)$$

This determines ϕ as a function of z and ϕ_L,

$$\phi(z) = \phi_L - P^{-1/2}\frac{S_1 K_1(\phi_L)}{2J(\phi_L)}(L-z)^2 + O(P^{-1}). \quad (34)$$

Based on (34), the constraint on the volume fraction (10) becomes

$$\bar{\phi} = \frac{1}{L}\int_0^L \left[\phi_L - P^{-1/2}\left(\frac{S_1 K_1(\phi_L)}{2J(\phi_L)}\right)(L-z)^2\right]dz + O(P^{-1}) = \phi_L - P^{-1/2}\left(\frac{S_1 K_1(\phi_L)}{2J(\phi_L)}\right)\frac{L^2}{3} + O(P^{-1}),$$

which gives

$$\phi_L = \bar{\phi} + P^{-1/2}\left(\frac{S_1 K_1(\phi_L)L^2}{6J(\phi_L)}\right) + O(P^{-1}) = \bar{\phi} + P^{-1/2}\frac{S_1 K_1(\bar{\phi})L^2}{6J(\bar{\phi})} + O(P^{-1}). \quad (35)$$

Substituting $z=0$ and $\phi=\phi_0$ into (33) we obtain

$$\sqrt{\phi_L - \phi_0} = P^{-1/4}\left(\frac{S_1 K_1(\phi_L)}{2J(\phi_L)}\right)^{1/2}L\left[1 + \frac{1}{3}P^{-1/2}\left(\frac{3J'(\phi_L)}{4J(\phi_L)} - \frac{K_1'(\phi_L)}{4K_1(\phi_L)}\right)\frac{S_1 K_1(\phi_L)}{2J(\phi_L)}L^2 + O(P^{-1})\right]. \quad (36)$$

Therefore, ϕ_0 can easily be determined from (35) and (36) and the result is

$$\phi_0 = \phi_L - (\phi_L - \phi_0) = \phi_L - \frac{S_1 K_1(\bar{\phi})L^2}{2J(\bar{\phi})}P^{-1/2} + O(P^{-1}) = \bar{\phi} - \frac{S_1 K_1(\bar{\phi})L^2}{3J(\bar{\phi})}P^{-1/2} + O(P^{-1}). \quad (37)$$

We can see from (35) and (37) that both ϕ_0 and ϕ_L are indeed close to $\bar{\phi}$ when the pressure is large. Therefore, our assumption that ϕ does not change significantly with z is indeed valid. Similarly, we expand ϕ near ϕ_L and integrate (29) to obtain

$$Q_0 = P^{5/4}\sqrt{2S_1}\rho^{-1/2}a[K_1(\phi_L)J(\phi_L)(\phi_L - \phi_0)]^{1/2}\left[1 - \left(\frac{J'(\phi_L)}{4J(\phi_L)} + \frac{K_1'(\phi_L)}{4K_1(\phi_L)}\right)(\phi_L - \phi_0) + O[(\phi_L - \phi_0)^2]\right]. \quad (38)$$

From (36) and (38), we get a simple relation between Q_0 and P,

$$Q_0 = \frac{S_1 aL}{\sqrt{\rho}}K_1(\bar{\phi})P = \frac{\mu L}{\rho a^2}K_1(\bar{\phi})P. \quad (39)$$

From (24), (37), and (39), we obtain

$$P^{1/2} = \left[w\sqrt{2\rho F(\bar{\phi})/\pi} + \left(\frac{F'(\bar{\phi})}{F(\bar{\phi})} - \frac{1}{\bar{\phi}}\right)\times\frac{S_1 K_1(\bar{\phi})L^2}{3J(\bar{\phi})}\right]\frac{w}{w_{\max} - w} \quad \text{for } w < w_{\max}, \quad (40)$$

where

$$w_{\max} = \frac{\mu L}{\rho a^2}K_1(\bar{\phi})F(\bar{\phi})/\bar{\phi}. \quad (41)$$

Therefore, a nontrivial steady state can be achieved only when the wall velocity is below $w_{\max}$.

In Fig. 4, we compare the asymptotic solution with the

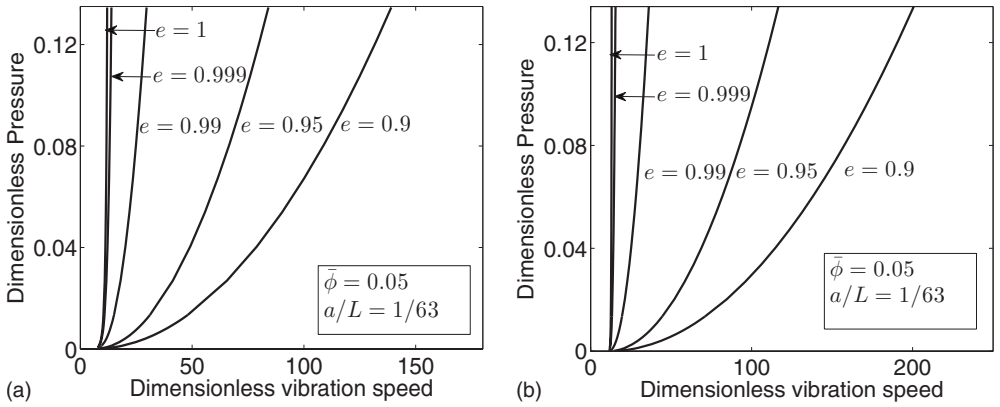

FIG. 5. The dimensionless pressure $P/(\frac{\mu^2 L^4}{\rho a^6})$ is plotted against the dimensionless wall velocity $w/(\frac{\mu L}{\rho a^2})$ for $\bar{\phi}=0.05$. Inelasticity in the collisions has a dramatic effect on the steady state of the systems when $w>w_{\max}$. For $e=1$, the dimensionless critical vibration speed $w_{\max}/(\frac{\mu L}{\rho a^2})=13.5$. (a) Maxwellian approximation near boundaries and constitutive laws (A1)–(A6); (b) the Brey *et al.* [2] model near boundaries and constitutive laws (A7)–(A16).

general solution for the same parameters used in Fig. 3. The dots are the asymptotic solution for the dimensionless pressure, the solid curve is the general solution and the dashed line is the location of the maximum dimensionless vibration speed $w_{\max}/(\frac{\mu L}{\rho a^2})$. It shows that the asymptotic solution is in good agreement with the general solution when the pressure is large.

IV. THEORETICAL PREDICTIONS FOR INELASTIC-PARTICLE SYSTEMS

In the preceding section, we have shown that, when inelastic effects are neglected and $w<w_{\max}$, the fluid drag can dissipate energy sufficiently rapidly to balance the energy input from the vibrating boundary and give a steady state. However, when $w>w_{\max}$, neglecting inelastic effects leads the system pressure to continuously increase and no steady-state solution exists. Therefore, we must include the effects of inelastic collisions when $w>w_{\max}$.

When the collisions between particles are not elastic, energy dissipation of the system will be caused not only by drag, but also inelasticity. We show that the latter will play a critical role in the energy dissipation when $w>w_{\max}$. Relative to the elastic situation, the system will be less energetic given the same amount of external energy since particles will lose more energy due to inelastic-particle-particle collisions and inelastic-particle-boundary collisions. We will show that systems with inelastic particles behave very differently from systems with elastic particles. The inelastic-particle system is determined by Eqs. (10), (14)–(16), (19), and (20). Following the same integration procedure as in Sec. III A, i.e., multiplying both sides of (14) by $J(\phi)\frac{d\phi}{dz}$ and performing integration from ϕ to ϕ_L, we get

$$J(\phi)\frac{d\phi}{dz} = \sqrt{2}[I_1(\phi,\phi_L,P) + I_2(\phi,\phi_L,e) + I_3(\phi_L,e_w)]^{1/2}, \tag{42}$$

where

$$I_1(\phi,\phi_L,P) = \int_{\phi}^{\phi_L} P^{-1/2} S_1 K_1(\phi') J(\phi') d\phi',$$

$$I_2(\phi,\phi_L,e) = \int_{\phi}^{\phi_L} (1-e^2) S_2 K_2(e,\phi') J(\phi') d\phi',$$

and

$$I_3(\phi_L,e_w) = \frac{1}{2}\left(\frac{1-e_w^2}{\sqrt{2\pi}a}\frac{\phi_L}{F^{3/2}(\phi_L)}\right)^2.$$

The quantities I_1, I_2, and I_3 are related to energy loss associated with viscosity, inelastic collisions between particles, and inelastic collisions between particles and boundaries, respectively.

For $e<1$, we cannot determine the solution in a simple parametric form and we must resort to numerical methods. The results are shown in Fig. 5 for $\bar{\phi}=0.05$. In this case, the dimensionless critical vibration speed for systems with $e=1$ is $w_{\max}/(\frac{\mu L}{\rho a^2})=13.5$. Figure 5 shows that inelastic effects give rise to the existence of steady states for values of $w>w_{\max}$. In Fig. 6 we plot the local volume fraction against the distance from the vibrating wall. Figure 6 shows that in this case, $\phi(z)$ is relatively insensitive to P, but is not uniform in z. This is in sharp contrast to the case of elastic-particle systems in which particles distribute almost uniformly for large P, see Fig. 3. In the case of elastic particles, the drag plays a decreasingly important role in controlling the dynamics and so the temperature and the local volume fraction become uniform. However, for inelastic particles the loss of energy due to collisions plays an important role no matter how large the pressure. Therefore, as one moves away from the vibrating boundary, inelastic collisions cause the temperature to decrease. Since the pressure is constant, this means that the local volume fraction must increase.

We now analyze the asymptotic behavior of pressure in the inelastic-particle system for large w since we are interested in what will happen when the vibration speed exceeds the critical value $w_{\max}$ after the inelastic effects are included.

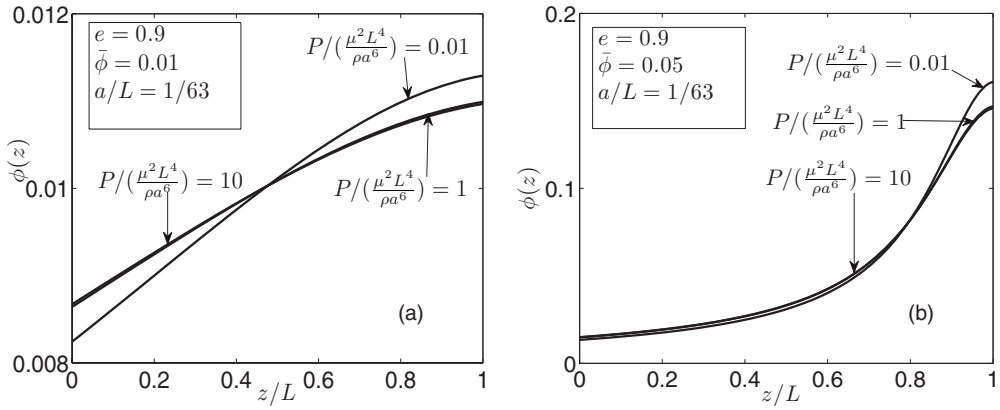

FIG. 6. The local volume fraction $\phi(z)$ is plotted against z/L for inelastic-particle systems ($e=0.9$) for various pressures. (a) $\bar{\phi}=0.01$; (b) $\bar{\phi}=0.05$. The volume fraction profile is insensitive to changes in pressure when the pressure is large. There is a large variation in the volume fraction at different z locations. This is in sharp contrast to the elastic-particle systems in which the volume fraction is uniform in z when the pressure is large. The constitutive model (A1)–(A6) is used for both (a) and (b).

In particular, we will show analytically that for large values of w the steady-state solution still exists. This is in contrast to the elastic-particle system. We will also show that P is proportional to w^2.

We note that for an inelastic system, namely $e<1$ and $e_w<1$, the term I_1 is negligible in comparison with the terms I_2 and I_3 for large P. After evaluating (42) at $z=0$, and substituting the result into (16), we obtain

$$\frac{Q_0}{P^{3/2}} = \left(\frac{2a^2}{\rho}[I_2(\phi_0,\phi_L,e) + I_3(\phi_L,e_w)]\right)^{1/2}. \tag{43}$$

From (20), we obtain

$$\frac{Q_0}{P^{3/2}} = \frac{1+e_w}{2}\frac{\phi_0}{F(\phi_0)}\left((1+e_w)\sqrt{\frac{\rho F(\phi_0)}{2\pi}}r^2 + e_w r - (1-e_w)\sqrt{\frac{2}{\pi\rho F(\phi_0)}}\right), \tag{44}$$

where $r=\frac{w}{\sqrt{P}}$. Equating (43) and (44) gives us

$$\left(\frac{2a^2}{\rho}[I_2(\phi_0,\phi_L,e) + I_3(\phi_L,e_w)]\right)^{1/2} = \frac{1+e_w}{2}\frac{\phi_0}{F(\phi_0)}\left((1+e_w)\sqrt{\frac{\rho F(\phi_0)}{2\pi}}r^2 + e_w r - (1-e_w)\sqrt{\frac{2}{\pi\rho F(\phi_0)}}\right). \tag{45}$$

Equation (45) is a quadratic equation in r and we denote the only positive root as $r(\phi_0,\phi_L)$. Therefore,

$$P = \frac{w^2}{r^2(\phi_0,\phi_L)}. \tag{46}$$

We note that the quantity $r(\phi_0,\phi_L)$ only depends on ϕ_0 and ϕ_L. In general, ϕ_0 and ϕ_L depend on $\bar{\phi}$ and P. However, for sufficiently large values of w, P will be large and so the volume fraction profile $\phi(z)$ will be insensitive to P as can be seen from large P limit of (42). That is ϕ_0 and ϕ_L will only depend on $\bar{\phi}$. In this case, r also only depends on $\bar{\phi}$.

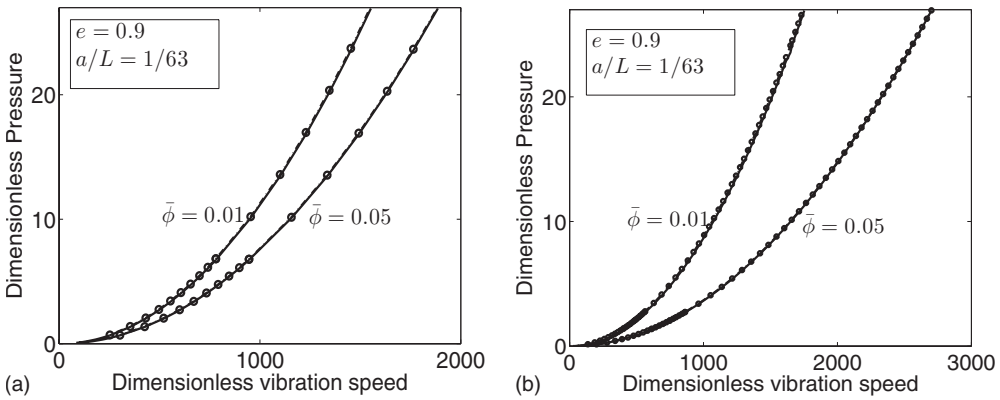

FIG. 7. The dimensionless pressure $P/(\frac{\mu^2 L^4}{\rho a^6})$ is plotted against the dimensionless wall velocity $w/(\frac{\mu L}{\rho a^2})$ for inelastic-particle systems ($e=0.9$) and various mean volume fractions. The asymptotic solution (dots) approximate the exact solution (solid curve) well. The singularity in the elastic system with $w>w_{\max}$ is removed once the effects of inelastic collision are included. (a) Maxwellian approximation near boundaries and constitutive laws (A1)–(A6); (b) the Brey *et al.* [2] model near boundaries and constitutive laws (A7)–(A16).

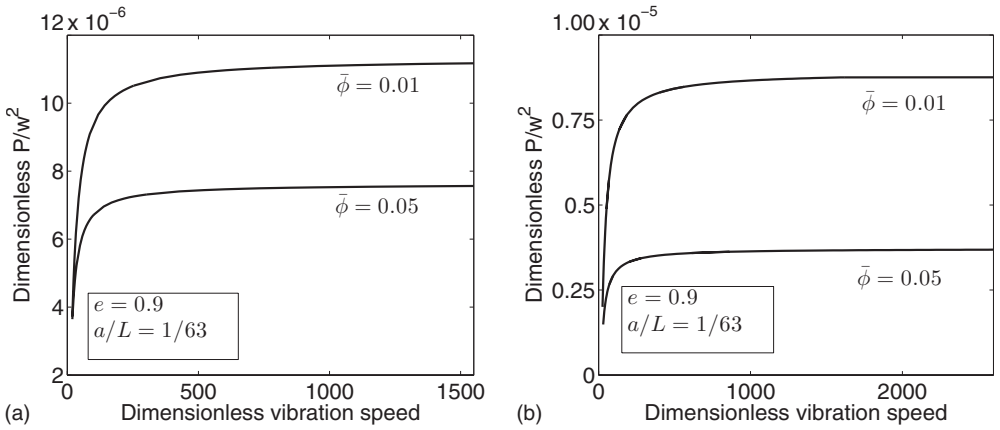

FIG. 8. The dimensionless P/w^2 is plotted against the dimensionless wall velocity $w/(\frac{\mu L}{\rho a^2})$. P is proportional to w^2 under large pressure. (a) Maxwellian approximation near boundaries and constitutive laws (A1)–(A6); (b) the Brey *et al.* [2] model near boundaries and constitutive laws (A7)–(A16).

In Fig. 7 we plot the dimensionless pressure against the dimensionless wall velocity and compare the asymptotic (dots) and numerically obtained solutions (solid curves). The agreement is excellent over a range of mean volume fractions. In Fig. 8 we plot P/w^2 against w and show that P/w^2 indeed tends to a constant for large w. For all values of w, the steady state exists and the pressure does not tend to infinity for any finite vibration speed. Therefore, the singularity that occurs at $w=w_{\max}$ in the elastic case is removed once the effects of inelastic collisions are included.

Intuitively, one would expect that, as $\bar{\phi}$ increases, more particles collide with the vibrating boundary, then both pressure and energy flux should increase. Figure 9 shows that this is indeed true for elastic particles. However, Fig. 9 also shows that the pressure and energy flux are not monotonic functions of $\bar{\phi}$ for $e<1$. The intuition given above is only correct for dilute systems in which collisions between particles are negligible. This is why, in Fig. 9, both the pressure and the energy flux increase with $\bar{\phi}$ when $\bar{\phi}$ is small. However, as $\bar{\phi}$ increases further, the inelastic collisions play a critical role in dissipating energy which leads to lowering the pressure and energy flux. As $\bar{\phi}$ increases further, the particles become more packed, and the energy dissipation does not grow as fast as the energy input. Then the pressure becomes an increasing function of $\bar{\phi}$ again. Therefore, the nonmonotonic behavior shown in Fig. 9 is due to the interplay between two effects: An increase in $\bar{\phi}$ leads to an increase in energy input due to collisions with the vibrating boundary, but also leads to more energy dissipation due to inelastic collisions.

Figure 5 shows that the behavior in inelastic-particle systems is dramatically different from that in elastic-particle systems. To understand such phenomenon, we consider an extremely simple system in which there is only one particle in the system. Due to the drag any velocity components in the horizontal directions will tend to zero and the particles will eventually move vertically back and forth between the two walls. Suppose a particle begins from the bottom boundary with vertical velocity V_0 and no horizontal velocity. The particle will move up to the top wall with drag, experience an inelastic collision with the fixed boundary, bounce back from it and move to the bottom wall. Then it gets more energy from the vibrating wall. We will refer to this sequence as a "cycle." If collisions are elastic, the loss of energy only depends on the drag μ and the distance L between the two

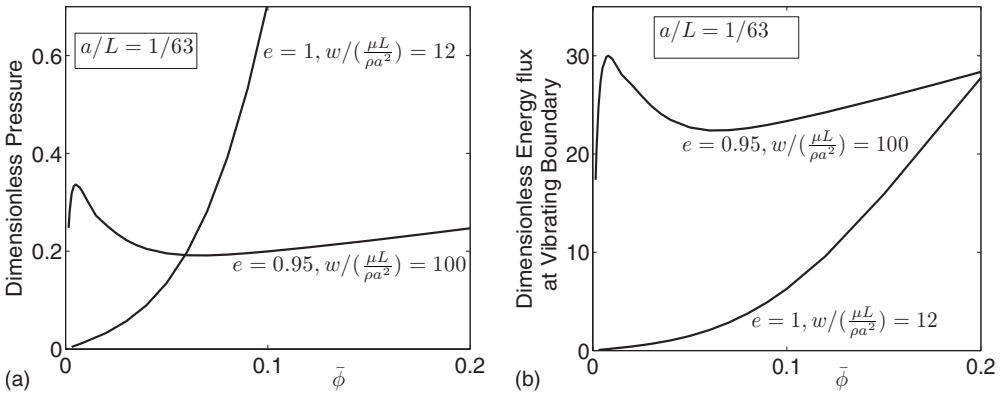

FIG. 9. (a) The dimensionless pressure $P/(\frac{\mu^2 L^4}{\rho a^6})$ and (b) the dimensionless energy flux at vibrating boundary, $Q_0/(\frac{\mu^3 L^5}{\rho^2 a^8})$, are plotted against the mean volume fraction. For inelastic-particle systems, they are not monotonically increasing as $\bar{\phi}$ increases. The Maxwellian approximation near boundaries and constitutive laws (A1)–(A6) are used in both (a) and (b).

boundaries. Let V_n be the velocity of the particle after the nth cycle. After the first cycle, the velocity becomes $V_1=V_0+2w-2\hat{w}$, where $\hat{w}=\frac{9\mu L}{2\rho a^2}$. Hence $V_n=V_{n-1}+2w-2\hat{w}=V_0+2n(w-\hat{w})$ after the nth cycle. In addition, the velocity V_0 must be greater than $2\hat{w}$ in order to guarantee that the particle collides with vibrating boundary after the first cycle, and the same requirement holds for V_n. It is easy to see that, in the limit $n\to\infty$, we have,

$$V_\infty=\begin{cases}0 & \text{if } w<\hat{w},\\ V_0 & \text{if } w=\hat{w},\\ \infty & \text{if } w>\hat{w}.\end{cases}$$

The above expression shows that there exists a finite critical vibration speed $\hat{w}=\frac{9\mu L}{2\rho a^2}$ which adds a suitable amount of energy to the system to compensate exactly for the energy loss caused by drag. Either lower or higher vibration speeds will result in the particle stopping or the energy growing without bound, respectively.

In the single-particle model with an elastic particle, a nontrivial steady state only exists for a single value of the wall velocity. In the multiparticle system the nontrivial steady state exists for a range of wall velocities. The difference is because particle scattering from interparticle collisions means that particles do not travel a fixed distance. Interparticle collisions also give a distribution of particle velocities.

Now we include the effects of inelastic collisions with the walls in our simple single-particle system. In the single-particle system, there is no energy loss from particle-particle collisions, but collisions with boundaries reduce the energy in the system. The reduction of the velocity during one cycle due to drag is fixed. Whereas, the reduction of the velocity during one cycle due to inelasticity is proportional to the velocity. Therefore, drag alone may not be able to dissipate the energy gained from the vibrating wall, while the inelasticity can. For elastic particles, this is why the steady state does not exist for values of the wall velocity above a critical value. While for inelastic particles, the steady state does exist no matter how large the wall velocity is.

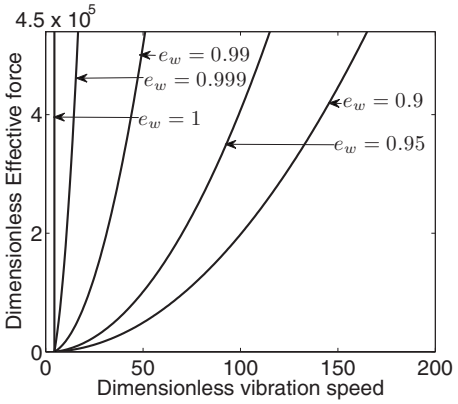

FIG. 10. The dimensionless effective force $F/(\frac{\mu^2 L}{\rho a})$ is plotted against the dimensionless wall velocity $w/(\frac{\mu L}{\rho a^2})$ for the single-particle system. The simple single-particle system indeed captures the main features of multiparticle systems.

A simple analysis shows that the initial vertical velocity V_0 must be greater than $\frac{1+e_w}{e_w}\hat{w}$ in order to complete the first cycle, and after a large number of cycles the velocity tends to

$$V_\infty=\frac{w-e_w\hat{w}}{1-e_w}. \tag{47}$$

Therefore, as long as $w>\frac{1}{e_w}\hat{w}$, a steady-state solution always exists. Equation (47) can be rewritten as $w=\hat{w}+(1-e_w)(V_\infty-\hat{w})$. The first term is the same as in the elastic case, and the second term $(1-e_w)(V-\hat{w})$ represents the additional energy input needed to compensate for the energy loss due to the inelastic collisions.

Based on the velocity V_∞ at steady state, one can easily obtain the change of momentum and the time spent in each cycle. The ratio of these two quantities gives the effective force on the walls,

$$F=\begin{cases}\dfrac{12\pi\mu a\hat{w}}{\ln\dfrac{V_0}{V_0-2\hat{w}}} & \text{for } e_w=1, w=\hat{w} \text{ and } V_0>2\hat{w},\\ \dfrac{6\pi\mu a(w+\hat{w})}{\ln\dfrac{e_w(w-e_w\hat{w})}{e_w w-\hat{w}}} & \text{for } e_w<1, w>\hat{w}/e_w \text{ and } V_0>\dfrac{1+e_w}{e_w}\hat{w},\\ 0 & \text{for } w<\hat{w}/e_w \text{ or } V_0<\dfrac{1+e_w}{e_w}\hat{w}.\end{cases} \tag{48}$$

It is easy to show that for inelastic-particle systems, the force given by (48) is asymptotically proportional to w^2. This is exactly the same qualitative behavior that we have analyzed for inelastic multiparticle systems, see Eq. (46).

In Fig. 10, we show the dimensionless force $F/(\frac{\mu^2 L}{\rho a})$ as a function of dimensionless vibration speed $w/(\frac{\mu L}{\rho a^2})$ at various

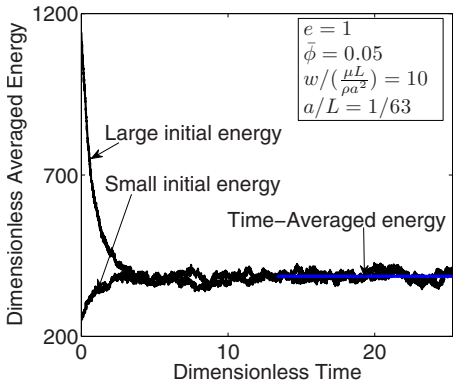

FIG. 11. (Color online) The dimensionless averaged energy $[\text{energy}/(\frac{\mu^2 L^2}{\rho a})]$ is plotted against dimensionless time $(\text{time}/\frac{\rho a^2}{\mu})$ for elastic-particle systems $(e=1)$ with $\bar{\phi}=0.05$, $w/\frac{\mu L}{\rho a^2}=10$, and $a/L=1/63$. The averaged energy at steady state does not depend on the initial state of the system.

values of e_w for the simple single-particle system. By comparing Figs. 5 and 10, one sees that single-particle systems indeed capture the main features of multiparticle systems.

V. VERIFICATION BY NUMERICAL SIMULATIONS

To verify the theoretical predictions that we have presented in the Secs. III and IV, we perform direct numerical simulations in three dimensions. The implementation of the simulations is straightforward. Between collisions, the particles move under Newton's second law. We use an approach similar to that used by Valiveti and Koch [23] that can be applied to a wide variety of particle systems with drag. We therefore use a fixed time step and perform a collision check after each step. If any collisions occur during the time step, the algorithm uses Newton's second law to compute the time of collision and the velocities and positions of the involved particles at the time of collision. The particle velocities are updated with the standard collision rules. The velocities at the end of the time step are then computed. In addition an underlying mesh is used to achieve a fast detection of particle collisions.

We choose the following parameters for the system in our simulation: $a/L=1/63$. In Fig. 11, we show that the system indeed reaches a steady state and the state is independent of initial energy in the system as long as the initial energy is sufficiently large.

Figure 12 shows the relation between dimensionless $P/(\frac{\mu^2 L^4}{\rho a^6})$ and $w/(\frac{\mu L}{\rho a^2})$ for $e=1$. The results from simulations are shown as circles and the theoretical predictions based on the Maxwellian approximation at the boundaries are shown as solid curves. The theoretical predictions based on the more detailed analysis of the boundary conditions given in [2] are shown as dashed curves. Even though the full simulated system is very complicated, our simple theoretical model captures all of the essential features. Our theoretical analysis in Sec. IV demonstrated that it is critical to include the effects of inelastic collisions when $w>w_{\max}$. In Fig. 13, we show the dimensionless pressure as a function of the dimensionless vibration speed in an inelastic-particle system with $\bar{\phi}=0.0361$ and various values of e. Figure 13 shows that the steady state indeed exists in the numerical simulations with inelastic particles. Figure 13 also shows that our theoretical predictions for the pressure based on the Maxwellian approximation (solid curves) and that based on the Brey *et al.* [2] approximation (dashed curves) are in qualitatively good agreement with the results from numerical simulations (circles). It shows that the theoretical predictions for the qualitative behavior of the system are generic, and do not depend on the details of the approximation for the velocity distribution near the boundaries.

VI. EFFECTS OF NONLINEAR DRAG

In Sec. III we showed that order of magnitude estimates can lead one to neglect inelastic effects. When inelastic effects are neglected, we showed that linear drag can provide

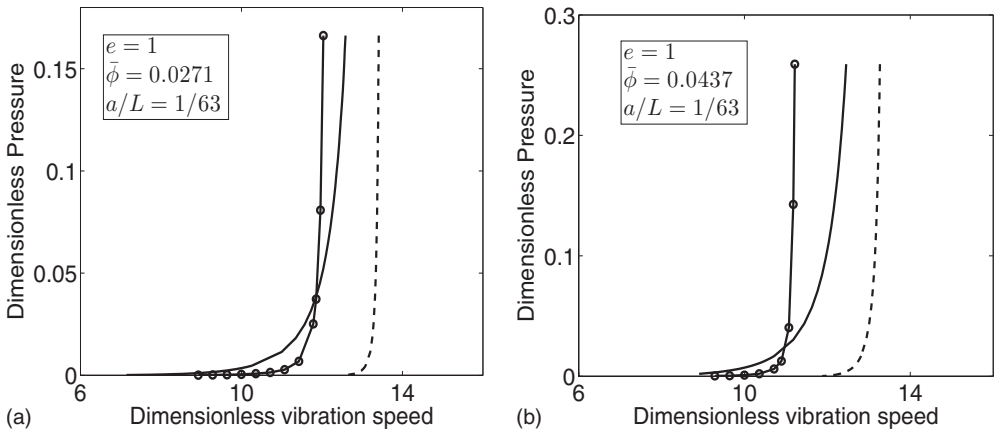

FIG. 12. The dimensionless pressure $P/(\frac{\mu^2 L^4}{\rho a^6})$ is plotted against the dimensionless vibration speed $w/(\frac{\mu L}{\rho a^2})$ for elastic-particle systems $(e=1)$ and various mean volume fractions. The theoretical predictions [solid curves for the Maxwellian approximation near boundaries and constitutive laws (A1)–(A6) and dashed curves for the Brey *et al.* [2] model near boundaries and constitutive laws (A7)–(A16)] behave qualitatively the same as the results from numerical simulations (circles). All results showed that no steady state exists above a certain critical vibration speed.

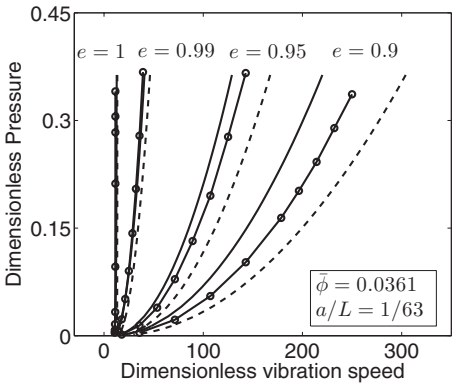

FIG. 13. The dimensionless pressure $P/(\frac{\mu^2 L^4}{\rho a^6})$ is plotted against the dimensionless vibration speed $w/(\frac{\mu L}{\rho a^2})$ for $\bar{\phi}=0.0361$ and various values of e. The theoretical predictions [solid curves for the Maxwellian approximation near boundaries and constitutive laws (A1)–(A6) and dashed curves for the Brey *et al.* [2] model near boundaries and constitutive laws (A7)–(A16)] behave qualitatively the same as the results from numerical simulations (circles).

sufficient dissipation to give a bounded steady state if the wall speed is below a critical value $w_{\max}$. On the other hand, if the wall speed exceeds a critical value, then the dissipation from a linear drag cannot match the rate of energy input and the kinetic energy of the particles grows without bound. For values of wall speed exceeding the critical value, the inclusion of inelastic effects prevents this unbounded growth in the kinetic energy even though order of magnitude estimates suggest that inelastic effects are negligible. In this section, we show that nonlinear drag effects can play a similar role to that played by inelastic effects. That is, order of magnitude estimates can lead one to neglect nonlinear drag effects, but if one does indeed neglect these effects, then unbounded growth in the kinetic energy can occur. However, if one does not neglect the nonlinear drag effects such unbounded growth can never occur.

An order of magnitude estimate would lead one to neglect nonlinear drag effects if

$$\mathrm{Re} = \frac{\rho_f a w}{\mu} \ll 1.$$

In Sec. III we showed that the critical value of the wall velocity occurs when $\frac{\rho a^2 w}{\mu L} = O(10)$. For values of the wall speed near this critical value

$$\mathrm{Re} = \frac{\rho_f a w}{\mu} = \frac{\rho_f}{\rho}\frac{L}{a}\frac{\rho a^2 w}{\mu L} = \frac{\rho_f}{\rho_p}\frac{L}{a}O(10).$$

If we consider metal particles suspended in a gas at normal atmospheric pressures, we typically have density ratios $\rho_f/\rho = O(10^{-4})$, so if $L/a = O(10^2)$, order of magnitude estimates would indeed lead one to neglect nonlinear drag terms. However, we know from Sec. III that such an assumption can lead to unbounded growth in the kinetic energy for elastic-particle systems. Therefore, we need to include the effects of inertia. We note that the nonlinear drag terms become more important for dense, highly pressurized gases.

There is an extensive literature relating to the effects of fluid inertia on flows through fixed beds of particles. This dates back to the pioneering work of Ergun [24] and has been further developed by numerous authors [25–31]. However, the effects of fluid inertia on suspensions has received much less attention [32,33]. Nevertheless, for $\mathrm{Re} = O(10)$ or less results from numerical simulations [32] show that the viscous dissipation can be well modeled by the functional form

$$\Gamma_{\mathrm{vis}} = \frac{\mu T}{a^2}\left(\Gamma_1(\phi) + \Gamma_3(\phi)\frac{\rho_f a T^{1/2}}{\mu}\right). \tag{49}$$

Therefore, the total dissipation $\Gamma_{\mathrm{vis}} + \Gamma_{\mathrm{inelast}}$ can be written in the form

$$\Gamma_{\mathrm{vis}} + \Gamma_{\mathrm{inelast}} = \Gamma_1(\phi)\frac{\mu}{a^2}T + \left((1-e^2)\Gamma_2(e,\phi) + \frac{\rho_f}{\rho}\Gamma_3(\phi)\right)\frac{\rho}{a}T^{3/2}. \tag{50}$$

Hence, the dissipation due to the nonlinear component of the drag and the dissipation due to inelasticity have the same $T^{3/2}$ scaling behavior. In fact, the system with nonlinear drag and inelasticity is identical to the system with linear drag and an effective coefficient of restitution $\hat{e}(e,\phi)$ that is given by solving

$$(1-\hat{e}^2)\Gamma_2(\hat{e},\phi) = (1-e^2)\Gamma_2(e,\phi) - \frac{\rho_f}{\rho}\Gamma_3(\phi). \tag{51}$$

Alternatively, the system with nonlinear drag and inelasticity is also identical to the system with elastic particles, but with an effective dissipation from the nonlinear component of the drag $\hat{\Gamma}_3$ given by

$$\hat{\Gamma}_3(e,\phi) = \Gamma_3(\phi) + (1-e^2)\frac{\rho}{\rho_f}\Gamma_2(e,\phi). \tag{52}$$

We note that this equivalence between inelastic collisions and nonlinear drag has been discussed in a previous study [32].

In what follows, we determine the relation between the pressure P and the wall velocity w for inelastic-particle systems with nonlinear drag using the Maxwellian approximation for the energy input at the walls. After substituting the relation $\rho F(\phi)T = P$ into (6) with Γ_{vis} given by (49), we have

$$-\frac{d}{dz}\left(J(\phi)\frac{d\phi}{dz}\right) = P^{-1/2}S_1K_1(\phi) + (1-e^2)S_2K_2(e,\phi) + S_3K_3(\phi), \quad z \in (0,L), \tag{53}$$

where S_1, S_2, $K_1(\phi)$, and $K_2(e,\phi)$ are given by (17),

$$S_3(\phi) = \frac{\rho_f}{\rho a^2} \tag{54}$$

and

$$K_3(\phi) = \frac{\Gamma_3(\phi)}{F^{3/2}(\phi)}. \tag{55}$$

The inelastic-particle system with nonlinear drag is determined by Eqs. (10) and (53) with the boundary conditions (15), (16), (19), and (20). Multiplying both sides of (53) by $J(\phi)\frac{d\phi}{dz}$ and performing integration from ϕ to ϕ_L, we get

$$J(\phi)\frac{d\phi}{dz} = \sqrt{2}[I_1(\phi,\phi_L,P) + I_2(\phi,\phi_L,e) + I_3(\phi_L,e_w) + I_4(\phi,\phi_L)]^{1/2}, \tag{56}$$

where $I_1(\phi,\phi_L,P)$, $I_2(\phi,\phi_L,e)$, and $I_3(\phi_L,e_w)$ are defined in (42), and

$$I_4(\phi,\phi_L) = \int_{\phi}^{\phi_L} S_3 K_3(\phi') J(\phi') d\phi'. \tag{57}$$

The quantities I_1 and I_4 are related to energy loss associated with linear and nonlinear drag, respectively. Whereas, the quantities I_2 and I_3 are related to energy loss associated with inelastic collisions between particles, and inelastic collisions between particles and boundaries, respectively. After evaluating (56) at $z=0$, and substituting the result and the expression for Q_0 given by (20) into (16), we obtain

$$\left(\frac{2a^2}{\rho}[I_1(\phi_0,\phi_L) + I_2(\phi_0,\phi_L,e) + I_3(\phi_L,e_w) + I_4(\phi_0,\phi_L)]\right)^{1/2} = \frac{1+e_w}{2}\frac{\phi_0}{F(\phi_0)}\left((1+e_w)\sqrt{\frac{\rho F(\phi_0)}{2\pi}}\frac{w^2}{P} + e_w\frac{w}{P^{1/2}} - (1-e_w)\sqrt{\frac{2}{\pi\rho F(\phi_0)}}\right). \tag{58}$$

For given e, e_w, ϕ_0, and ϕ_L, this equation determines P as a function of w. We now determine the asymptotic behavior of P when w is large. Since I_1 is proportional to $P^{-1/2}$ while I_2, I_3, and I_4 are independent of P, I_1 is negligible in comparison to I_2, I_3, and I_4 for large P. In this case, the inelastic collisions and nonlinear drag give the same order of magnitude contribution in the energy dissipation and the asymptotic behavior of P is given by

$$P = \frac{w^2}{s^2(\phi_0,\phi_L)}, \tag{59}$$

where $s(\phi_0,\phi_L)$ is the solution for the following equation:

$$\left(\frac{2a^2}{\rho}[I_2(\phi_0,\phi_L,e) + I_3(\phi_L,e_w) + I_4(\phi_0,\phi_L)]\right)^{1/2} = \frac{1+e_w}{2}\frac{\phi_0}{F(\phi_0)}\left((1+e_w)\sqrt{\frac{\rho F(\phi_0)}{2\pi}}s^2 + e_w s - (1-e_w)\sqrt{\frac{2}{\pi\rho F(\phi_0)}}\right). \tag{60}$$

Therefore, we have shown that both inelastic collisions and nonlinear drag can provide sufficient energy dissipation to form a steady state even for large value for w.

VII. CONCLUSIONS

In this paper, we have conducted a detailed study of the steady states of particle systems driven by a vibrating boundary. There are two factors contributing to the energy dissipation: The drag from interstitial fluid and inelastic collisions between particles. For systems with linear drag, our theoretical analysis showed that neglecting the effects of inelasticity in collisions is only possible when the vibration speed of the boundary is below a critical value. Above this critical speed, energy dissipation due to linear drag alone is not enough to dissipate the energy gained from the vibrating boundary. In this case, the pressure in the system continuously increases and no steady state exists. Therefore, one must include the effects of inelastic collisions and/or the effects of nonlinear drag if the wall speed exceeds the critical value. We showed that a steady state always exists in inelastic-particle systems and the pressure is asymptotically proportional to the square of vibration speed of the boundary. We have confirmed our theoretical predictions by numerical simulations, and the results from numerical simulations are in qualitatively good agreement with our theoretical predictions. We have also showed that nonlinear drag effects in the dissipation can play a similar role as inelasticity in preventing the kinetic energy growing without bound.

ACKNOWLEDGMENT

This work is supported by the Research Grants Council of the Hong Kong Special Administrative Region, China, Contract No. CityU 103205.

APPENDIX A: CONTINUUM MODELS

Continuum models that relate the energy flux, dissipation, and pressure to the state of the system have been derived by a number of authors, under different assumptions. These different models give slightly different functional forms for the quantities Γ_1, Γ_2, F, κ_1, and η_1 in Eqs. (2), (3), and (7)–(9). In this paper we will illustrate our results by using the same two constitutive models used by Martin *et al.* [7].

Various authors have assumed that $1-e \ll 1$ and derived expressions that account for the effects of high packing fractions. Jenkins [20] gave expressions for κ_1 and η_1 used in the energy flux,

$$\kappa_1(e,\phi) = \frac{8}{\pi^{1/2}}\phi^2\chi\left[1 + \frac{9\pi}{32}\left(1 + \frac{5}{12\phi\chi}\right)^2\right] \tag{A1}$$

and

$$\eta_1(e,\phi) = 0, \tag{A2}$$

where

$$\chi = \frac{1 - \phi/2}{(1-\phi)^3}. \tag{A3}$$

This should be supplemented by an expression for F used in the kinetic pressure given by Carnahan and Starling [34],

$$F(\phi) = \phi(1 + 4\phi\chi). \tag{A4}$$

The expression for Γ_1 used in the viscous dissipation has been derived by Sangani *et al.* [16],

$$\Gamma_1(\phi) = \frac{27\phi}{2} R_{\text{diss}}, \tag{A5}$$

where R_{diss} is a factor that accounts for increased dissipation that occurs due to the pressure of neighbors. An approximate expression that fits the result of numerical simulations was given in Sangani *et al.* [16]. In this paper we neglect this effect and set $R_{\text{diss}}=1$, although this does not qualitatively affect all figures presented in our numerical demonstration. The expression for Γ_2 used in the inelastic dissipation is given by Jenkins and Savage [19],

$$\Gamma_2(e,\phi) = \frac{6\phi^2\chi}{\sqrt{\pi}}. \tag{A6}$$

Brey *et al.* [17,18] derived expressions that neglect the effects of high packing fractions, but include high-order corrections in e. In this low volume fraction limit, the relevant expressions are

$$\Gamma_1(\phi) = \tfrac{27}{2}\phi, \tag{A7}$$

$$\Gamma_2(e,\phi) = \frac{6\phi F(\phi)}{\sqrt{\pi}}\left(1 + \frac{3}{32}c(e)\right), \tag{A8}$$

$$\kappa_1(e,\phi) = \kappa^*(e)\frac{25\sqrt{\pi}}{64}, \tag{A9}$$

$$\eta_1(e,\phi) = \eta^*(e)\frac{25\sqrt{\pi}}{64\phi}, \tag{A10}$$

and

$$F(\phi) = \phi(1 + 4\phi\chi), \tag{A11}$$

where

$$\kappa^*(e) = \tfrac{2}{3}[1 + c(e)][\upsilon(e) - 2\zeta(e)]^{-1}, \tag{A12}$$

$$\eta^*(e) = 2\zeta(e)\left(\kappa^*(e) + \frac{c(e)}{3\zeta(e)}\right)[2\upsilon(e) - 3\zeta(e)]^{-1}, \tag{A13}$$

$$c(e) = \frac{32(1-e)(1-2e^2)}{81 - 17e + 30e^2(1-e)}, \tag{A14}$$

$$\zeta(e) = \tfrac{5}{12}(1-e^2)\left[1 + \tfrac{3}{32}c(e)\right], \tag{A15}$$

and

$$\upsilon(e) = \frac{1}{3}(1+e)\left(1 + \frac{33(1-e)}{16} + \frac{(19-3e)c(e)}{1024}\right). \tag{A16}$$

These constitutive laws given by Brey *et al.* [17,18] keep only the leading order contributions in ϕ and so one is naturally led to take the leading order expression for F, namely $F(\phi)=\phi$. When using the Maxwellian approximation near the boundaries, this represents no problem, but when using the Brey *et al.* [2] model for the boundary flux one obtains an expression for the asymptotic behavior of P near $w_{\max}$ (B10) that cancels if the leading order expression is used. Therefore, it is consistent to keep the higher-order terms for F in (A11), while discarding the higher-order terms for the other quantities. That is, in the $\phi\to 0$ limit, the contributions from the higher-order terms associated with quantities other than $F(\phi)$ vanish, but the higher-order terms associated with $F(\phi)$ are nonvanishing. This choice of constitutive law is similar to that used by Martin *et al.* [7].

We note that the expressions of Brey *et al.* [18] have been extended to higher densities by Garzo and Dufty [35] using revised Enskog theory.

APPENDIX B: THEORETICAL PREDICTIONS BASED ON A DETAILED ANALYSIS OF DISTRIBUTION AT BOUNDARIES

A number of authors including Warr *et al.*, Kumaran, McNamara, and Barrat, and McNamara and Luding have considered the problem of how to deal with the boundary conditions (17) and (18). The most detailed and complete study was performed by Brey *et al.* [2] who showed that the addition of energy causes significant deviations from the Maxwellian distribution for the vertical component of velocity in the vicinity of the wall. They recognized that a complete theoretical description of the distribution function could only be carried out in the context of the kinetic equation. Rather than dealing with the complexities of the kinetic equation, they proposed a simple and physically appealing model and found good agreement with Monte Carlo simulations. In this section, we will follow a similar approach to that given by Brey *et al.* and show that this approach gives results that have the same qualitative behavior as the ones based on the Maxwellian approach shown in Secs. II–IV. Following [2], we assume that the distribution function f_0 can be factorized as $f_0(\mathbf{u})=f_{xy}(u_x,u_y)f_z(u_z)$, where u_x, u_y, and u_z denote the components of velocity in the horizontal directions x, y and the vertical direction z, respectively. Here, f_{xy} and f_z are the probability density functions for the velocity in the horizontal directions and the vertical direction, respectively. Therefore, the energy flux at the vibrating boundary becomes

$$\begin{aligned} Q_0 &= \rho\phi_0 \int_{\mathbf{u}\cdot\hat{\mathbf{z}}<0} -\frac{u_z}{2}\{[(1+e_w)w - e_w u_z]^2 - u_z^2\} f_0(\mathbf{u}) d\mathbf{u} \\ &= \rho\phi_0 \int_{u_z<0} -\frac{u_z}{2}\{[(1+e_w)w - e_w u_z]^2 - u_z^2\} f_z(u_z) du_z, \end{aligned} \tag{B1}$$

since $\int_{u_x}\int_{u_y} f_{xy}(u_x,u_y)du_y du_x = 1$. Therefore, only $f_z(u_z)$ for $u_z<0$ matters in the evaluation of (B1). Any distribution f_z can be expressed as

$$f_z(u_z) = f^-(u_z) I_{u_z<0} + f^+(u_z) I_{u_z>0}.$$

Due to the motion of the wall and inelastic-particle collisions with the wall, f^+ is related to f^- by the following relation:

$$u_z f^-(u_z) I_{u_z<0} du_z = [(1+e_w)w - e_w u_z] f^+[(1+e_w)w - e_w u_z] I_{u_z<0} d[(1+e_w)w - e_w u_z],$$

which leads to

$$f^+(u)du = -\frac{(1+e_w)w-u}{e_w^2 u} f^-\left(\frac{(1+e_w)w-u}{e_w}\right)du \quad \text{for } u > (1+e_w)w.$$

Hence f_z becomes

$$f_z(u) = f^-(u) I_{u<0} - \frac{(1+e_w)w-u}{e_w^2 u} f^-\left(\frac{(1+e_w)w-u}{e_w}\right) I_{u>(1+e_w)w}. \tag{B2}$$

Substituting (B2) into (B1), we obtain

$$Q_0 = \frac{1+e_w}{2}\rho\phi_0[(1+e_w)w^2 f_1 + 2e_w w f_2 - (1-e_w)f_3], \tag{B3}$$

where $f_i = \int_{-\infty}^0 (-u)^i f^-(u)du$ for $i=1,2,\ldots$. Following Brey *et al.* [2], we match the energy of the particles at the boundary with the energy in the interior and assume that the horizontal components of the velocity are not significantly affected by the wall. This gives,

$$T_0 = (1+e_w)(wf_1 + f_2). \tag{B4}$$

Using $\rho F(\phi_0)T_0 = P$ to eliminate the temperature from (B4), we obtain

$$P = \rho F(\phi_0)(1+e_w)(wf_1 + f_2). \tag{B5}$$

Equations (B3) and (B5) give us a relation between Q_0 and P,

$$Q_0 = P\frac{\phi_0}{F(\phi_0)}\left(\frac{1+e_w}{2}w - \frac{1-e_w}{2}\frac{wf_2+f_3}{wf_1+f_2}\right). \tag{B6}$$

A similar approach can be used at the fixed boundary. By setting $w=0$, we get the energy flux at the fixed boundary, $z=L$,

$$Q_L = P\frac{\phi_L}{F(\phi_L)}\frac{1-e_w}{2}\frac{\tilde{f}_3}{\tilde{f}_2}, \tag{B7}$$

where $\tilde{f}_i = \int_0^\infty u^i \tilde{f}^+(u)du$ and $\tilde{f}^+$ is the distribution for $u_z>0$ at $z=L$.

For elastic-particle systems, i.e., $e=e_w=1$, we obtain

$$w = \frac{Q_0}{P}\frac{F(\phi_0)}{\phi_0}, \tag{B8}$$

and $Q_L=0$.

We comment that in Brey *et al.* [2], a specific functional form

$$f^-(u) = c_1 e^{-(u/k)^2} \tag{B9}$$

is used, and they only considered the case of $e_w=1$. Here we have showed that the approach of Brey *et al.* gives a simple relation (B8) for all functional forms of f^- when $e_w=1$. In other words, (B8) is independent of the functional form of f^- when $e_w=1$.

Based on the approach of Brey *et al.* [2], the elastic-particle system is governed by the same set of equations for the approach based on the Maxwellian approximation except that (24) is replaced by (B8), namely, it is governed by (10), (21)–(23), and (B8). Following the same procedure shown in Sec. III, the parametric solutions for P, $\bar{\phi}$, and Q_0, in terms of ϕ_0 and ϕ_L, are given by (26), (28), and (30), respectively. The wall velocity, w is related to ϕ_0 and ϕ_L by (B8).

The numerical results of this approach have been presented in Sec. III along with the approach based on the Maxwellian approximation near the boundaries. Both approaches have the same qualitative behavior. In particular, both approaches show that there exists a critical vibration speed above which no steady state exists in elastic-particle systems.

Following the same procedure given in Sec. III, the approach of Brey *et al.* gives the following expressions for the asymptotic behavior of P near $w_{\max}$:

$$P^{1/2} = \left(\frac{F'(\bar{\phi})}{F(\bar{\phi})} - \frac{1}{\bar{\phi}}\right)\left(\frac{S_1 K_1(\bar{\phi})L^2}{3J(\bar{\phi})}\right)\frac{w}{w_{\max}-w}, \tag{B10}$$

where

$$w_{\max} = \frac{\mu L}{\rho a^2}K_1(\bar{\phi})F(\bar{\phi})/\bar{\phi}. \tag{B11}$$

This expression for $w_{\max}$ given by (B11) is the same as (41) derived from the approach of Maxwellian approximation.

Based on the model of Brey *et al.* [2], the inelastic-particle systems, $e<1$ and $e_w<1$, are determined by (10), (14)–(16), and (B5)–(B7) and the functional form (B9) proposed in Ref. [2]. From (10), (14)–(16), (B7), and (B9), we have the following asymptotic expressions for $Q_0/P^{3/2}$ in terms of ϕ_0 and ϕ_L when w is large:

$$\frac{Q_0}{P^{3/2}} = \left(\frac{2a^2}{\rho}[I_2(\phi_0,\phi_L,e) + \tilde{I}_3(\phi_L,e_w)]\right)^{1/2}, \tag{B12}$$

where

$$\tilde{I}_3(\phi_L,e_w) = I_3(\phi_L,e_w)\frac{\pi^3 b_3^2}{4e_w(1+e_w)^2 b_2^3},$$

and $b_n = \int_0^\infty x^n e^{-x^2}dx$ for $n=1,2\ldots$. From (B5) and (B6), we have

$$\frac{Q_0}{P^{3/2}} = \frac{\phi_0}{\sqrt{4(1+e_w)\rho F^3(\phi_0)}}\frac{(1+e_w)w^2 f_1 + 2e_w w f_2 - (1-e_w)f_3}{(wf_1+f_2)^{3/2}} = \frac{\phi_0[(1+e_w)r^2 b_1 + 2e_w r b_2 - (1-e_w)b_3]}{\sqrt{4(1+e_w)\rho F^3(\phi_0)}(rb_1+b_2)^{3/2}} \times \left[\int_{-\infty}^0 e^{-x^2}\left(1 - \frac{x}{(1+e_w)r - e_w x}\right)dx\right]^{1/2}, \tag{B13}$$

where $r = \frac{w}{k}$. Equating (B12) and (B13) gives us

$$\left(\frac{2a^2}{\rho}[I_2(\phi_0,\phi_L,e)+\tilde{I}_3(\phi_L,e_w)]\right)^{1/2} = \frac{\phi_0[(1+e_w)r^2b_1+2e_wrb_2-(1-e_w)b_3]}{\sqrt{4(1+e_w)\rho F^3(\phi_0)}(rb_1+b_2)^{3/2}} \times\left[\int_{-\infty}^{0} e^{-x^2}\left(1-\frac{x}{(1+e_w)r-e_wx}\right)dx\right]^{1/2}. \quad \text{(B14)}$$

Solving (B14) gives us an expression of r in terms of ϕ_0 and ϕ_L, which we denote as $r(\phi_0,\phi_L)$. Substituting this value into (B5), we obtain

$$P = C_2(\phi_0,\phi_L)w^2, \quad \text{(B15)}$$

where

$$C_2(\phi_0,\phi_L) = \frac{\rho F(\phi_0)(1+e_w)}{r^2(\phi_0,\phi_L)}[r(\phi_0,\phi_L)b_1+b_2] \times\left[\int_{-\infty}^{0} e^{-x^2}\left(1-\frac{x}{(1+e_w)r(\phi_0,\phi_L)-e_wx}\right)dx\right]^{-1}.$$

Equation (B15) shows P is asymptotically proportional to w^2. This behavior is the same as (46) obtained from the approach based on the Maxwellian approximation.

[1] C. Bizon, M. D. Shattuck, J. B. Swift, and H. L. Swinney, Phys. Rev. E **60**, 4340 (1999).
[2] J. J. Brey, M. J. Ruiz-Montero, and F. Moreno, Phys. Rev. E **62**, 5339 (2000).
[3] J. Eggers, Phys. Rev. Lett. **83**, 5322 (1999).
[4] V. Kumaran, Phys. Rev. E **57**, 5660 (1998).
[5] J. Lee, Physica A **219**, 305 (1995).
[6] J. Lee, Physica A **238**, 129 (1997).
[7] T. W. Martin, J. M. Huntley, and R. D. Wildman, J. Fluid Mech. **535**, 325 (2005).
[8] S. McNamara and J. L. Barrat, Phys. Rev. E **55**, 7767 (1997).
[9] S. Warr and J. M. Huntley, Phys. Rev. E **52**, 5596 (1995).
[10] J. J. Wylie and D. L. Koch, Phys. Fluids **12**, 964 (2000).
[11] P. Biswas, P. Sanchez, M. R. Swift, and P. J. King, Phys. Rev. E **68**, 050301(R) (2003).
[12] N. Burtally, P. J. King, and M. R. Swift, Science **295**, 1877 (2002).
[13] M. C. Leaper, A. J. Smith, M. R. Swift, P. J. King, H. E. Webster, N. J. Miles, and S. W. Kingman, Granular Matter **7**, 57 (2005).
[14] J. J. Wylie, Q. Zhang, H. Y. Xu, and X. X. Sun, Europhys. Lett. **81**, 54001 (2008).
[15] J. J. Wylie and Q. Zhang, Phys. Rev. E **74**, 011305 (2006).
[16] A. S. Sangani, G. Mo, H.-K. Tsao, and D. L. Koch, J. Fluid Mech. **313**, 309 (1996).
[17] J. J. Brey, F. Moreno, and J. W. Dufty, Phys. Rev. E **54**, 445 (1996).
[18] J. J. Brey, J. W. Dufty, C. S. Kim, and A. Santos, Phys. Rev. E **58**, 4638 (1998).
[19] J. T. Jenkins and S. B. Savage, J. Fluid Mech. **130**, 187 (1983).
[20] J. T. Jenkins, *Physics of Dry Granular Media*, edited H. J. Herrman, J.-P. Hovi, and S. Luding (Kluwer, Dordrecht, 1999), pp. 353–370.
[21] I. Goldhirsch and G. Zanetti, Phys. Rev. Lett. **70**, 1619 (1993).
[22] J. J. Brey, M. J. Ruiz-Montero, and F. Moreno, Phys. Rev. E **63**, 061305 (2001).
[23] P. Valiveti and D. L. Koch, Phys. Fluids **11**, 3283 (1999).
[24] S. Ergun, Chem. Eng. Prog. **48**, 89 (1952).
[25] S. Rojas and J. Koplik, Phys. Rev. E **58**, 4776 (1998).
[26] J. S. Andrade, M. P. Almeida, J. Mendes Filho, S. Havlin, B. Suki, and H. E. Stanley, Phys. Rev. Lett. **79**, 3901 (1997).
[27] D. L. Koch and A. J. C. Ladd, J. Fluid Mech. **349**, 31 (1997).
[28] R. S. Maier, D. M. Kroll, Y. E. Kutovsky, H. T. Davis, and R. S. Bernard, Phys. Fluids **10**, 60 (1998).
[29] R. M. Fand, B. Y. K. Kim, A. C. C. Lam, and R. T. Phan, ASME Trans. J. Fluids Eng. **109**, 268 (1987).
[30] R. J. Hill, D. L. Koch, and A. J. C. Ladd, J. Fluid Mech. **448**, 213 (2001).
[31] R. J. Hill, D. L. Koch, and A. J. C. Ladd, J. Fluid Mech. **448**, 243 (2001).
[32] J. J. Wylie, D. L. Koch, and A. J. C. Ladd, J. Fluid Mech. **480**, 95 (2003).
[33] D. L. Koch and R. J. Hill, Annu. Rev. Fluid Mech. **33**, 619 (2001).
[34] N. F. Carnahan and K. E. Starling, J. Chem. Phys. **51**, 635 (1969).
[35] V. Garzo and J. W. Dufty, Phys. Rev. E **59**, 5895 (1999).